Simulation of regional features of the Indian summer monsoon in a GCM

R. S. Ajayamohan, B. N. Goswami[+], T.E. LaRow, S. Cocke and D. W. Shin

Center for Ocean-Atmospheric Prediction Studies, Florida State University, Tallahassee.

[+] *Centre for Atmospheric & Oceanic Sciences, Indian Institute of Science, Bangalore 560 012.*

Submitted to MWR

Corresponding author address:

R. S. Ajayamohan, Center for Ocean-Atmospheric Prediction Studies, Florida State University, Tallahassee, FL 32306-2840, USA. E-mail: ajayan@coaps.fsu.edu

ABSTRACT

Major characteristics of Indian summer monsoon climate are analyzed using simulations from the upgraded version of Florida State University Global Spectral Model (FSUGSM). The Indian monsoon has been studied in terms of mean precipitation and low-level and upper-level circulation patterns and compared with observations. In addition, model's fidelity in simulating monsoon intraseasonal and interannual variability and the teleconnection patterns associated with the monsoon interannual variability is examined.

The model is successful in simulating the major rainbelts over the Indian monsoon region. However, the model exhibits bias in simulating the precipitation bands over South China Sea and West Pacific region. Seasonal mean circulation patterns of low-level and upper-level winds are consistent with the model's precipitation pattern. Basic features like onset and peak phase of monsoon is realistically simulated. However, model simulation indicates an early withdrawal of monsoon. Northward propagation of rainbelts over the Indian continent is simulated fairly well, but over the ocean propagation is weak. Model simulates the meridional dipole structure associated with the monsoon intraseasonal variability realistically. Model is unable to capture the observed interannual variability of monsoon. Analysis of teleconnection patterns reveals models fidelity in simulating the component of interannual variability forced by sea surface temperature.

1. Introduction

The Indian summer monsoon (June-September, JJAS) precipitation is closely related to the annual evolution of the Tropical Convergence Zone (TCZ, Gadgil 2003; Ramage 1971; Shukla 1987) and is characterized by some unique regional features. It includes existence of two bands of maximum precipitation, one over the continent and north Bay-of-Bengal and the other over the Indian Ocean (IO) between the equator and 10°S, the narrow maximum along the Western Ghats with a rain shadow over the south eastern continent and the maximum over the head Bay-of-Bengal. Active and break spells of the Indian monsoon are unique regional features of monsoon intraseasonal oscillations (ISOs). The monsoon ISOs comprise of the 10-20 day westward propagating mode (Chatterjee and Goswami 2004; Chen and Chen 1993; Krishnamurti and Bhalme 1976) and the northward propagating 30-60 day mode (Goswami and Ajayamohan 2001; Sikka and Gadgil 1980; Webster et al. 1998; Yasunari 1979). The dominant monsoon ISOs has large spatial scale similar to that of the seasonal mean and its interannual variability (Goswami and Ajayamohan 2001; Sperber et al. 2001). The evolution of the annual cycle of the monsoon and the monsoon ISOs are, therefore, intimately linked (Gadgil 2003; Goswami and Ajayamohan 2001; Waliser et al. 2003).

Prediction of the seasonal monsoon precipitation assumes great importance as the agricultural production and water resources depend crucially on the precipitation during the rainy summer season (Gadgil 2003; LinHo and Wang 2002; Webster et al. 1998). However, almost all climate models have insignificant (nearly zero) skill in simulating the observed interannual variability of the summer seasonal mean precipitation over the Asian monsoon region (Brankovic and Palmer 2000; Kang et al. 2002; Wang et al. 2004). Ability of a climate model to simulate and predict the seasonal mean precipitation anomalies depends on three factors, namely its ability to simulate the observed climatological distribution of summer precipitation (systematic bias), its ability to simulate the forced mode of interannual variability associated with slow Sea Surface Temperature (SST)

variability such as that associated with the El Niño and Southern Oscillation (ENSO) and the model's ability to correctly simulate the internal Low Frequency (LF) variability. The internal LF variability, in turn, appears to be generated by the intraseasonal oscillations (Ajayamohan and Goswami 2003; Goswami 1998; Goswami and Ajayamohan 2001). Therefore, the ability of a model to simulate the regional features of summer mean precipitation and the climatology of the monsoon ISOs with an acceptable degree of fidelity is essential for it to be useful for prediction of the seasonal mean.

Although the climate models have improved over the last couple of decades in simulating the global climate in general, almost all climate models still have serious systematic bias in simulating the regional features of the Indian summer monsoon climate and its interannual variability (Gadgil and Sajani 1998; Kang et al. 2002; Sperber and Palmer 1996). Gadgil and Sajani (1998) carried out a detailed analysis of monsoon precipitation simulation by more than thirty models that participated in the Atmospheric Model Intercomparison Project (AMIP, Gates 1992). They found that a large number of models simulate exceptionally high precipitation over equatorial Indian Ocean and exceptionally low rainfall over the Indian continent. Even within the oceanic rainbelt, maximum precipitation is often simulated in the western IO rather than over the eastern IO, as observed. Even when some models simulate continental rainbelt, they do so between 10°N and 15°N, much southward compared to the observed position of about 25°N. Most models also simulate the narrow north-south oriented precipitation band along the Western Ghats as a broad blob extending too much to the Arabian Sea and fail to simulate the rain shadow over southeast India. Poor simulation of the climatological mean precipitation may also influence the model's ability to simulate the teleconnection pattern associated with ENSO SST variability and hence in simulating the global forced mode. Recently, Waliser et al. (2003) assessed the intraseasonal variability associated with the Asian summer monsoon for 10 GCMs. They have shown that many models lack in representing the intraseasonal variability in the equatorial Indian Ocean. Double convergence

zone about the equator, lack of eastward propagation are some of the major problems identified in the simulation of intraseasonal oscillations. Unrealistically high (low) ISO activity in a model can give rise to unrealistic simulation of internal LF variability and influence simulation of seasonal mean anomaly.

In the present study we investigate the ability of the recently upgraded FSUGSM (Cocke and LaRow 2000) in simulating the complex regional features of climatological mean Indian summer monsoon. In this context, we shall explore in detail the model's ability to simulate the seasonal mean monsoon precipitation, intraseasonal and interannual monsoon variability and the associated teleconnection patterns and compare with the observations. Section.2 gives a brief description of the model, design of the numerical experiments and the data sets used for the study. Section.3 shows the the Northern Hemisphere summer and winter climatology of the model and discusses its merits and demerits compared to observed climatologies. Section.4 considers the description on the model simulation of monsoon intraseasonal variability. Section.5 is the analysis of interannual variability of monsoon and it's teleconnection patterns. Main conclusions of this work is summarized in Section.6.

2. Experimental framework and data sources

FSUGSM is a global spectral model with T63 horizontal resolution ($\sim$1.86°) with 17 unevenly spaced σ-levels. The new version of the FSUGSM includes the option to select alternative parameterization schemes to the original ones, including most of the CCM3.6 physics package. In this experiment, we selected the following CCM3.6 physical parameterizations: PBL and vertical diffusion, shallow convection, large scale condensation, dry convective adjustment, and ocean surface flux routines. The land surface scheme, including the land surface flux parameterizations, are from the original FSUGSM. See Kiehl et al. (1998) for a complete description of CCM3.6 physical parametrization schemes.

Observed pentad and monthly precipitation datasets based on Climate Prediction

Centre Merged Analysis of Precipitation (CMAP; Xie and Arkin 1997) were used for validation of simulated precipitation. The National Centre for Environmental Prediction/National Centre for Atmospheric Research (NCEP/NCAR) daily and monthly reanalysis products (Kalnay et al. 1996) were used for validation of the circulation fields.

FSUGSM has recently been equipped with the option of incorporating any one of six different state-of-the-art cumulus parametrization schemes. They are (1) NCEP/SAS (National Centre for Environmental Prediction/Simplified Arakawa-Schubert; Pan and Wu 1994); (2) NCAR/ZM (National Center for Atmospheric Research; Zhang and McFarlane 1995); (3) NRL/RAS (Naval Research Laboratory/Relaxed Arakawa-Schubert; Rosmond 1992); (4) MIT (Massachusetts Institute of Technology; Emanuel and Zivkovic-Rothman 1999); (5) GSFC/RAS (Goddard Space Flight Center/Relaxed Arakawa-Schubert; Moorthi and Suarez 1992) and (6) modified KUO (Krishnamurti et al. 1983). In an effort to construct an optimum model for better simulation of the regional features of the Indian monsoon, we examined, how the Indian summer monsoon is simulated by the model with these different cumulus schemes. For that purpose a five member ensemble simulations for five months (May-September) with different initial conditions were carried out for two years (1987 and 1988). Initial conditions differ from each other by one day starting from May 1. The ensemble mean of 10 realizations (5 each for 1987 and 1988) of June-September (JJAS) mean precipitation for each scheme are compared with the observations (Fig.1). Observed precipitation (Fig.1(g)) is based on CMAP. The main drawback in most schemes is the inability of the model to simulate both the primary monsoon precipitation zone over the Indian continent and the secondary monsoon precipitation zone over the equatorial Indian Ocean together. KUO (Fig.1(e)), NCAR (Fig.1(b)), NRL (Fig.1(c)) overestimates precipitation over the Indian Ocean while NCEP (Fig.1(a)) and GSFC (Fig.1(d)) underestimates the precipitation over the Indian Ocean. NCEP, NCAR and NRL schemes simulates the two zones of precipitation as one zone resulting in above normal rainfall over the equator. Apart from that, all six schemes ex-

cept MIT (Fig.1(f)) fails to simulate the rain shadow region over the southern tip of the Indian peninsula. Position of the two major zones of precipitation is realistic in the MIT scheme, though the simulated rainfall over the foothills of Himalayas is slightly larger than observed. We find that FSUGSM with MIT scheme is able to simulate the unique regional features of the Indian monsoon region realistically and hence select this scheme for further analysis. Shin et al. (2003) also found that FSUGSM with MIT scheme produce better seasonal forecast over the Indian region. They have also shown that the MIT scheme is less sensitive to model resolution than any other scheme. We carry out a long integration (21 years;1982-2002) of the FSUGSM with the MIT convection scheme with observed weekly mean SST as boundary forcing. Weekly mean SST data is derived from Reynolds and Smith (1994). Daily model outputs are saved for evaluation of simulation of intraseasonal as well as interannual variability.

3. Simulation of Seasonal Mean

In this section, we investigate the fidelity of FSUGSM in simulating the observed climatological mean precipitation and circulation. The seasonal mean precipitation calculated from model simulations during the Northern Hemispheric summer and winter (Fig.2(a,b)) are compared with the observed seasonal mean precipitation (Fig.2(c,d)). For the summer monsoon season (JJAS), the simulation of precipitation maxima over the head Bay-of-Bengal (around 20°N) and west coast of India compare quite well with the corresponding observations. FSUGSM also succeeds in simulating the secondary precipitation maximum over the Indian Ocean. However, the model overestimates precipitation over Africa and Central America. Systematic error in simulation of JJAS climatological mean summer precipitation however, occurs over the South China Sea and the Western North equatorial Pacific (110°E to 140°E) where the model climate is too dry compared to the observed. Also the South Pacific Convergence Zone extends too far to the east in the model. The pattern correlation between simulated and observed precipitation clima-

tology in the tropics (0°-360° and 40°S-40°N) is 0.6. The simulated climate has a major systematic error during northern winter (DJF) over the Indian Ocean and Indonesian region. The rainbelt remains in the Northern Hemisphere between 5°N and 10°N instead of retreating to the southern hemisphere between 10°S and 5°S as in observations. We note that (not shown) the model's skill in simulating winter climatology is poor with all convection schemes. Thus the model captures the precipitation zones in summer months reasonably well but has systematic bias in simulating the observed precipitation zones realistically in the winter months.

The mean JJAS climatology of the Indian summer monsoon constructed from the 21-year simulations in terms of lower and upper level circulation are shown in Fig.3(a,b) while similar climatology of observed winds from NCEP/NCAR reanalysis are shown in Fig.3(c,d). The model simulates the geographical position of the low level jet, cross equatorial flow and the south equatorial easterlies realistically (Fig.3a and c). Consistent with the weaker simulated monsoon precipitation over the South China Sea region, the strength of the low-level winds are also weaker than the observed. The pattern correlation between simulated and observed zonal and meridional wind climatology at 850 hPa over the domain 40°-140°E;20°S-35°N are 0.88 and 0.64 respectively. FSUGSM underestimates the strength of the upper level easterly jet. The Tibetan anticyclone is simulated bit too far to the north and the easterly jet is weaker than observed in general with the maximum around 10°N rather than close to the equator as in observations (see Fig.3b and d). Also the simulated winds between the equator and 10°N are too zonal compared to the observed. The pattern correlation between simulated and observed zonal and meridional wind climatology at 200 hPa over the domain 40°-140°E;20°S-35°N are 0.94 and 0.56 respectively.

The model's ability in simulating the annual evolution of the Indian monsoon is tested in Figure 4. We select two indices to test the model's climatological annual evolution, one based on precipitation and the other that is directly linked to the dynam-

ics. Goswami et al. (1999) proposed an Extended range Indian Monsoon Rainfall index (EIMR) and claimed that it might yield a more comprehensive definition of the non-adiabatic heating associated with the Indian summer monsoon. They defined EIMR as the mean JJAS precipitation averaged over 70°-110°E and 10°-30°N, taking into account the fact that the oceans and nearby regions of India play an important role in the Indian summer monsoon variability. Since the low level winds over the Arabian Sea are strongly related to the precipitation over the monsoon region (Joseph and Sijikumar 2004), we constructed an index to represent Kinetic Energy (KE) of Low-Level Jet (KELLJ) defined as the seasonal mean KE of winds at 850hPa averaged over 50°-65°E and 5°-15°N. The annual evolution of EIMR and KELLJ calculated from the climatological mean of model simulations are compared with that calculated from the observed climatological mean (Fig.4). Except in August and September when the simulated precipitation is close to the observed precipitation, the model simulates higher precipitation than observed. The discrepancy is largest during dry winter months (November-April) when the model simulates significant precipitation over the Indian monsoon region. Sudden increase in kinetic energy associated with the onset of monsoon in early May is well captured by the model (Fig.4). Kinetic energy decreases in mid August, indicating an early withdrawal of monsoon. Though the model simulates the onset of monsoon realistically, it shows a systematic bias in simulating the withdrawal phase of the monsoon in September. This discrepancy which reflects in both the monsoon indices (EIMR and KELLJ) may be related to model's soil moisture parametrization.

The onset and withdrawal of the Indian monsoon are closely linked with changes in the sign of the large scale meridional gradients of pressure associated with the land-ocean contrast (Li and Yanai 1996). Vertically averaged temperature between 600 hPa and 200 hPa averaged over a large region in the north and another over the south are indicative of large scale pressures over the respective regions. North-south gradient of the vertically averaged (600hPa-200hPa) temperature from the model are compared with

temperature gradient calculated from the observations (Fig.5a,b). Solid line indicates the vertically averaged temperature over the northern latitudes (30°-130°E,10°N-40°N) and the dotted line represents vertically averaged temperature over the southern latitudes (30°-130°E,30°S-10°N). The reversal of the large scale temperature gradient correspond quite well with the onset and withdrawal phases of monsoon (Fig.5b). In terms of this large scale index, the onset and withdrawal of the Asian monsoon is simulated well by the model.

4. Simulation of Monsoon Intraseasonal Variability

The characteristics of the monsoon intraseasonal variability simulated by FSUGSM during the summer monsoon season (June-September) are validated with the corresponding observed monsoon intraseasonal characteristics. Daily anomalies of some fields (precipitation, zonal and meridional winds at 850hPa and 200hPa) were calculated by removing the annual cycle (defined as the annual mean + first two harmonics) from the daily data. A precipitation time series is constructed using daily anomalies between June 1 and September 30 for all 21 years averaged over a small region in the Bay-of-Bengal (85°-90°E,10°N-15°N) to examine the intraseasonal temporal characteristics of simulated precipitation anomalies. Similar time series for zonal wind at 850hpa (U_{850}) averaged over a small region in the Arabian Sea (60°-65°E,10°N-15°N) is also constructed and a power spectrum analysis is carried out on these two time series (Fig.6). The model simulated precipitation and U_{850} show statistically significant peaks with periods between 10 and 20 days and between 30 and 90 days. This is consistent with the observations (Goswami and Ajayamohan 2001; Krishnamurti and Bhalme 1976; Yasunari 1980). All the selected field anomalies are bandpass filtered using a Lanczos filter (Duchon 1979) to retain periodicities between 10 and 90 days for the period June 1 to September 30 for all the 21 years in order to study the spatial characteristics of the monsoon intraseasonal oscillations which include both these preferred periodicities. Realistic simulation

of intraseasonal precipitation variance is seen over the preferred locations of the TCZ like the Arabian Sea, Bay-of-Bengal and the South equatorial Indian Ocean (Fig.7a). However, model simulated intraseasonal variances over Arabia and some parts of Africa are higher than the observed intraseasonal precipitation variance (see Fig.7b). Model simulation of intraseasonal precipitation variance is poor over the eastern equatorial IO and equatorial West Pacific which is consistent with the systematic bias of the model's summer monsoon rainfall climatology. Over the Indian monsoon region, model simulates intraseasonal variance of low level zonal winds reasonably well (Fig.7c). However, U_{850} intraseasonal variance simulated over the Bay-of-Bengal is deficient when compared to observations (Fig.7d). Systematic bias of the model in simulating the western Pacific winds reflects in the simulation of much weaker intraseasonal variance of zonal winds over this region.

A reference time series is constructed by averaging 10-90 day filtered precipitation over EIMR (70°-110°E;10°-25°N) during the summer monsoon season (1 June to 30 September) for the period considered for the study (1982-2002) to evaluate model's fidelity in simulating the propagation characteristics of monsoon ISO. Lag regression of 10-90 day filtered precipitation anomalies are then calculated with respect to the reference time series both for the model simulations and for the observations. Regressed precipitation averaged over 70°-95°E is plotted as a function of latitude (Fig.8a,b). It is clear that the model simulates the northward propagation of monsoon ISO over the northern latitudes (Fig.8a). However, model shows a bias in simulating the propagation characteristics over the southern latitudes. Model propagation starts from the tip of the Indian peninsula (north of 8°N). This may be due to problems associated with the models boundary layer formulation over the ocean restricting it to produce less rainfall over the ocean. Systematic northward propagation from 5°S is seen in U_{850} of the observed ISOs (Fig.8d) while the simulated ISOs show northward propagation from about 5°N (Fig.8c) consistent with the propagation characteristics of the precipitation ISOs.

The phase composite analysis (Murakami and Nakazawa 1985) is used to find the large-scale spatial structure associated with the monsoon ISOs. We calculated daily precipitation composites for all active and break days for the period 1982-2002 from 1 June to 30 September. Active and break days are defined using a reference time series created based on EIMR; active days are those for which filtered precipitation anomalies are greater than +1 standard deviation, while those less than -1 standard deviation are termed as break days. Fig.9a shows the climatological mean active minus break precipitation composite for the 21-year period and Fig.9b represents the corresponding composite from observations. It is clear that the model simulates the meridional dipole structure associated with the Indian summer monsoon intraseasonal variability realistically. However, it may be noted that the simulated intraseasonal variability over the warm waters of equatorial Indian Ocean is weak compared to observations. Similarly, phase composite analysis carried out on 850hPa winds (Fig.10a) are compared with the corresponding phase composite based on observations (Fig.10b). A noteworthy feature of the spatial pattern of monsoon ISO involves enhancement (decrease) of monsoon low level winds in the active (break) phases of Indian summer monsoon. The model simulates the spatial pattern associated with the monsoon ISO for low-level winds similar to that of the observed except that the amplitude of model simulated winds are slightly weaker than that of the observed. Also, consistent with bias in the model climatology, model fails to capture the intraseasonal variability over the west Pacific. Similar composite plot for upper-level winds is shown in Fig.11. Easterlies over the continent and location of the Tibetan anticyclone are simulated realistically by the model.

Thus, the model is successful in simulating the temporal and spatial characteristics of observed monsoon ISO during the northern summer over the Indian region reasonably well. The next section examines the model's fidelity in simulating the monsoon interannual variability and it's associated teleconnection patterns.

5. Simulation of Monsoon Interannual Variability

Different monsoon indices are used to evaluate the strength of the monsoon rainfall over India and its Interannual Variability (IAV). Most commonly used index is the IMR (Indian Monsoon Rainfall index) defined as the precipitation averaged from June to September over India (Parthasarathy et al. 1994). This index is calculated based on data from 306 raingauge stations distributed uniformly through out India. It might be difficult to compare it directly with the simulated JJAS climatological mean precipitation averaged over the subcontinent. Hence, we use EIMR, precipitation averaged over 70°-110°E;10°-25°N as the rainfall index. Other indices used include KELLJ (defined in section.3) and Monsoon Hadley-Circulation Index, an index based on meridional wind shear (MH; Goswami et al. 1999). This broad-scale index represents the monsoon variability as V_{850}-V_{200}, where V_{850} and V_{200} are the meridional anomalies of 850hPa and 200hPa wind anomalies averaged for the JJAS season over 70°-110°E and 10°-25°N. Observed EIMR is based on CMAP dataset while NCEP winds are used to calculate KELLJ and MH. Fig.12a compares the model EIMR with CMAP EIMR. A first look at this plot suggests that the model simulation of precipitation amplitude is generally high. Model simulation of interannual variability is not reliable as it is unable to simulate the amplitudes of all the dry and wet years correctly. Fig.12b shows the different monsoon indices simulated by the model normalized by their own standard deviation. It is clear that there is a good correspondence between the indices within the model. Since we have only one realization of the long simulation, exact simulation the interannual variability may not be expected. Cross correlation between the different monsoon indices within the model and with the observations are summarized in Table-I. The correlation coefficient between EIMR and KELLJ is 0.85, while that of EIMR and MH is 0.5 and that between KELLJ and and MH is 0.59. This indicates that both the dynamical indices have good correlation with EIMR for FSUGSM. While comparing the model monsoon indices with the observed monsoon indices, it is seen that EIMR correlates poorly with

MH but has moderate positive correlation with KELLJ. The correlation coefficient between model KELLJ and observed KELLJ is 0.43. Model KELLJ also have moderate positive correlation with model EIMR.

We evaluate the interannual variance simulated by FSUGSM for the 21-year period taken for the study. Interannual precipitation variance simulated by the model (Fig.13a) for the northern summer monsoon season is compared with the corresponding interannual variance calculated from the observed data set (Fig.13b). Model simulation of interannual variance over the Indian monsoon region is reasonable when contrasted with the CMAP variance. Model succeeds in simulating interannual variance over the preferred zones of precipitation. However, the large interannual variance over Western and Central equatorial Pacific seen in the observations are not captured by the model. Similarly, comparison of interannual variance associated with low-level zonal winds with the variance calculated from observations reveal that the model overestimates interannual variance over the equatorial Indian Ocean and underestimates variance over the West Pacific (Fig.13c,d).

To find the large scale spatial structure associated with the simulated IAV of the summer monsoon, composite of precipitation and lower and upper level winds corresponding to strong and weak monsoon are calculated. Strong (weak) monsoons are identified based on normalized EIMR from model simulations and observed datasets. Strong (weak) monsoon years are identified as those years where the normalized EIMR is greater than 1 standard deviation (less than -1 std). The climatological mean strong minus weak monsoon composites of the simulated precipitation, low-level and upper-level winds (Fig.14a,c,d) are compared with the corresponding composites from observations (Fig.14b,d,f). We can identify some similarities in the spatial structure of IAV of precipitation from model simulations and observations over the continent. Model simulates the West coast rainfall, maxima over the Bay-of-Bengal and the rainshadow region over the Southeast India realistically. Systematic error of the model in simulating the west

Pacific rainfall reflects in the simulation of IAV also. In the Indian Ocean region, model simulates the rainbelt as an elongated patch from 40°E to 120°E. Observations show an east-west dipole structure in this region. This bias is reflected in the simulation of IAV of 850hPa winds (see Fig.14c) as the south easterlies over the equatorial Indian Ocean is not captured by the model. Model simulates the 200hPa easterlies over the Indian Ocean region but fails to simulate it over the Indian continent when compared to observations (Fig.14d,f).

The above analysis clearly indicates the fact that the model exhibits poor skill in the simulation of IAV of Indian summer monsoon. The question is whether the poor skill of simulation of IAV of monsoon is due to the systematic problem of the model or due to problems inherent with the IAV of monsoon system. Simulation of IAV of Indian monsoon is one of the most intriguing problems (Gadgil 2003; Gadgil et al. 2002). In this context, it might be interesting to look into how the model responds to observed forced variability associated with the SST variations.

Impact of air-sea interaction associated with the changes in the Walker circulation induced by changes in the convection between Indian and Pacific Oceans are well known. Several studies have shown the significant ENSO-monsoon relationship on interannual time scales (Ju and Slingo 1995; Webster et al. 1998). Most of these studies indicate a close relationship between droughts of the Indian monsoon and El Niño. However, there seems to be a break down in this relationship in the recent decade (Krishakumar et al. 1995). To assess model's performance in simulating interannual variations of Indian summer monsoon, it is important to ascertain some of models teleconnection patterns. Moreover, teleconnection analysis is used here as a measure of model's ability to correctly simulate the component of interannual variability forced by the imposed boundary conditions. First, we examine the correlation coefficients between simulated northern summer monsoon precipitation and Niño-3 Sea Surface Temperature Anomalies (SSTA), a popular index used to quantify strength of ENSO signal. Lag-zero correlation map of

JJAS Niño-3 SSTA with the simulated JJAS precipitation (Fig.15a) is compared with the correlation map of Niño-3 SSTA with CMAP precipitation (Fig.15b). Model simulates the ENSO related precipitation variability realistically. Precipitation over the Indian continent and Niño-3 SSTA are significantly negatively correlated indicating the ENSO-Monsoon signal in the model simulations. However, observed correlation map (Fig.15b) indicates a weaker relationship, possibly due to the break down of ENSO-Monsoon relationship in the recent decade. Another interesting difference to note when contrasted with observations is the positive correlation of equatorial Indian Ocean precipitation with Niño-3 SSTA. This means that an increase in the SST in the eastern Pacific is associated with an increase in precipitation over the eastern equatorial IO. This helps in further reduction of precipitation over the Indian monsoon region through induced subsidence. This is consistent with simulated stronger drying over the Indian continent associated with the ENSO compared to observations.

Further, we examine how the Walker and monsoon Hadley (MH) circulation associated with ENSO are simulated by the FSUGSM. For this purpose, JJAS averaged zonal, meridional and pressure vertical velocity anomalies were regressed with JJAS mean Niño-3 SST. Fig.16a shows the anomalous monsoon Hadley circulation pattern associated with ENSO simulated by FSUGSM represented by regressions of meridional wind and pressure vertical velocity (with a negative sign) averaged over 70°-90°E and Fig.16c shows the anomalous Walker circulation pattern simulated represented by regressions of zonal wind and pressure vertical velocity (with a negative sign) averaged over a domain 5°S-5°N. Fig.16c,d shows the corresponding Walker and monsoon Hadley circulation pattern associated with ENSO from observations. The simulated MH circulation shows a clear anomalous meridional cell with ascending motion between the equator and 10°S and a descending motion between 10°N and 30°N. An interesting feature is a rather shallow meridional circulation cell between 5°S and 15°N. The observed MH circulation has ascending motion spreading from 5°S to 12°N and weaker descending motion between 12°N

and 25°N. The anomalous Walker cell associated with the ENSO with ascending motion in the eastern Pacific and descending motion in the western Pacific (Fig.16d) is simulated well by the model (Fig.16c) except that the descending motion around 120°E is much weaker at lower levels. Moreover, the model simulates a much stronger ascending motion over the IO (Fig.16c) compared to the observations (Fig.16d).

6. Summary and Discussion

Using simulations from the upgraded version of FSUGSM, major characteristics of Indian summer monsoon climate is studied and validated with the observed data sets. In addition to assessing the simulation of mean summer monsoon rainfall and it's associated circulation patterns, the fidelity of the model in reproducing the monsoon seasonal cycle, intraseasonal variability, interannual variability and associated teleconnection patterns are also investigated.

FSUGSM is able to simulate the unique regional features associated with the Indian summer monsoon realistically. The model produces a reasonable representation of the seasonal mean monsoon precipitation and circulation features although the amplitude of the simulated precipitation and circulation is higher than the observed. The major precipitation bands over the monsoon domain, one over the continent and Bay-of-Bengal and the other over the warm waters of the Indian Ocean are realistically simulated. The rainshadow region over the southeastern tip of the peninsula and the narrow maximum along the Western Ghats are simulated correctly. However, the model shows systematic bias in simulating the rainbands over south China Sea region and western north Pacific. These biases reflect in the simulated lower and upper level winds. Though the model succeeds in simulating the onset phase of Indian summer monsoon correctly, the withdrawal phase is simulated 30 days earlier than observed.

The model simulates temporal and spatial characteristics associated with the intraseasonal variability of the Indian monsoon with reasonable accuracy. Power spectrum

analysis carried out on model simulated precipitation and low level zonal wind anomalies show statistically significant peaks between 10 and 20 days and between 30 and 90 days similar to observations. Spatial structure of active and break phases of Indian summer monsoon simulated by the model are similar to that seen in the observations. However, the low level winds simulated by the model is too zonal over the equatorial Indian Ocean compared to observations. This discrepancy is reflected in the simulation of precipitation and 200hPa winds also. Northward propagation of intraseasonal anomalies are restricted over the land in the model simulations unlike the observations. Some characteristics of the monsoon intraseasonal oscillations are related to ocean-atmosphere coupling in the Indian Ocean and hence the intraseasonal variability of the model may be improved by coupling the model with ocean. Recently Rajendran et al. (2004) have shown that coupling over the Indian Ocean improves the simulation of monsoon intraseasonal oscillations.

With a single realization of the simulation, the model is not expected to simulate the observed interannual variability of the seasonal mean precipitation over the Indian monsoon region well. However, we find that the model also does not simulate the observed spatial structure of interannual variability of the monsoon well. Model simulates the rainbelt over the equatorial Indian Ocean as an elongated patch and fails to capture the east-west dipole structure of precipitation seen in observations over this region. It is to be noted that most dynamical models fail to capture the interannual variability associated with the Indian summer monsoon. This may be partly related to the systematic errors of the model simulations outside the Indian monsoon region. This may also be partly due to the fact that the predictability of the Indian summer monsoon is limited by internal variability whose amplitude over this region is comparable to that of the forced variability arising from slowly varying boundary forcings. Teleconnection analysis of the IAV of the Indian summer monsoon reveal models fidelity in simulating the component of IAV forced by sea surface temperature. Model simulates the ENSO related precipitation variability

reasonably well. ENSO-monsoon relationship is bit stronger in the model than observed. Ascending cell of Walker circulation due to warming of equatorial Pacific is simulated well. However, the descending cell over 120°E is weak in the model while the ascending motion over the Indian Ocean is stronger than observed in the model simulations.

By experimenting with a number of cumulus parametrization schemes, we find that the FSUGSM with the MIT convective scheme simulates the regional features of the summer mean precipitation over the Indian monsoon region well. However, it has been found to be at the cost of having significant systematic bias in simulating the precipitation over the western Pacific during northern summer and over the Indian Ocean and Indonesia during northern winter. The dry bias over the warm waters of the western Pacific during northern summer while simulating the precipitation over the Indian region correctly and the tendency of the rainbelt not to move to the warm waters of southern equatorial Indian Ocean during northern winter indicate certain deficiency in the coupling between the marine boundary layer and the cumulus scheme. Early withdrawal of the monsoon also indicates that some improvement is required in the land surface scheme. Work on these aspects is expected to improve the problem of systematic bias of the model.

Acknowledgment. Computations were performed on IBM SP4 at the FSU. COAPS receives its base support from the Applied Research Center, funded by NOAA Office of Global Programs awarded to Dr. James J. O'Brien. Prince K Xavier and R. Vinay IISc, Bangalore are acknowledged for many useful and lively discussions.

REFERENCES

Ajayamohan, R. S., and B. N. Goswami, 2003: Potential predictability of the Asian summer monsoon on monthly and seasonal time scales. *Met. Atmos. Phys.*, **84**, 83–100.

Brankovic, C., and T. N. Palmer, 2000: Seasonal skill and predictability of ECMWF PROVOST ensembles. *Quart. J. Roy. Meteor. Soc.*, **126**, 2035–2067.

Chatterjee, P., and B. N. Goswami, 2004: Structure, genesis and scale selection of the tropical quasi-biweekly mode. *Quart. J. Roy. Meteor. Soc.*, p. to appear.

Chen, T.-C., and J.-M. Chen, 1993: The 10-20-day mode of the 1979 Indian monsoon: Its relation with the time variation of monsoon rainfall. *Mon. Wea. Rev.*, **121**, 2465–2482.

Cocke, S., and T. E. LaRow, 2000: Seasonal predictions using a regional spectral model embedded within a Coupled Ocean-Atmospheric Model. *Mon. Wea. Rev.*, **128**, 689–708.

Duchon, C. E., 1979: Lanczos filtering on one and two dimensions. *J. Appl. Meteor.*, **18**, 1016–1022.

Emanuel, K. A., and M. Zivkovic-Rothman, 1999: Development and evaluation of a convective scheme for use in climate models. *J. Atmos. Sci.*, **56**, 1766–1782.

Gadgil, S., 2003: The Indian monsoon and it's variability. *Annu. Rev. Earth Planet. Sci.*, **31**, 429–467.

Gadgil, S., and S. Sajani, 1998: Monsoon precipitation in the AMIP runs. *Climate Dyn.*, **14**, 659–689.

Gadgil, S., J. Srinivasan, R. S. Nanjundiah, A. A. M. K. Krishan Kumar, and K. R. Kumar, 2002: On forecasting the Indian summer monsoon: the intriguing season of 2002. *Curr. Sci.*, **83**, 394–403.

Gates, W. L., 1992: AMIP: The Atmospheric Model Intercomparison Project. *Bull. Amer. Meteor. Soc.*, **73**, 1962–1970.

Goswami, B. N., 1998: Interannual variations of Indian summer monsoon in a GCM: External conditions versus internal feedbacks. *J. Climate*, **11**, 501–522.

Goswami, B. N., and R. S. Ajayamohan, 2001: Intraseasonal oscillations and interannual variability of the Indian summer monsoon. *J. Climate*, **14**, 1180–1198.

Goswami, B. N., V. Krishnamurthy, and H. Annamalai, 1999: A broad-scale circulation index for interannual variability of the Indian summer monsoon. *Quart. J. Roy. Meteor. Soc.*, **125**, 611–633.

Joseph, P. V., and S. Sijikumar, 2004: Intraseasonal variability of the low-level jet stream of the Asian summer monsoon. *J. Climate*, **17**, 1449–1458.

Ju, J., and J. Slingo, 1995: The Asian summer monsoon and ENSO. *Quart. J. Roy. Meteor. Soc.*, **121**, 1133–1168.

Kalnay, E., et al., 1996: The NCEP/NCAR 40-year reanalysis project. *Bull. Amer. Meteor. Soc.*, **77**, 437–471.

Kang, I. S., et al., 2002: Intercomparison of the climatological variations of Asian summer monsoon precipitation simulated by 10 GCMs. *Climate Dyn.*, **19**, 383–395.

Kiehl, J. T., J. J. Hack, G. B. Bonan, B. A. Bivile, D. L. Williamson, and P. J. Rasch, 1998: The National Centrer for Atmospheric Research Community Climate Model: CCM3. *J. Climate*, **11**, 1131–1149.

Krishakumar, K., M. K. Soman, and K. Rupakumar, 1995: Seasonal forecasting of Indian summer monsoon rainfall. *Weather*, **50**, 449–467.

Krishnamurti, T. N., and H. N. Bhalme, 1976: Oscillations of monsoon system. part I: Observational Aspects. *J. Atmos. Sci.*, **45**, 1937–1954.

Krishnamurti, T. N., S. Low-Nam, and R. Pasch, 1983: Cumulus parmetrization and rainfall rates (II). *Mon. Wea. Rev.*, **111**, 815–828.

Li, C., and M. Yanai, 1996: The onset and interannual variability of the Asian summer monsoon in relation to land-sea thermal contrast. *J. Climate*, **9**, 358–375.

LinHo, and B. Wang, 2002: The time-space structure of the Asian-Pacific summer monsoon: A fastannual cycle view. *J. Climate*, **15**, 2001–2019.

Moorthi, S., and M. J. Suarez, 1992: Relaxed Arakawa-Schubert: A parameterization of moist convection for General Circulation Models. *Mon. Wea. Rev.*, **120**, 978–1002.

Murakami, T., and T. Nakazawa, 1985: Tropical 45 day oscillations during 1979 Northern Hemisphere summer. *J. Atmos. Sci.*, **42**, 1107–1122.

Pan, H. L., and W. S. Wu, 1994: Implementing a mass flux convective parametrization scheme for the NMC medium-range forecast model. *Tenth Conference on Numerical Weather Prediction Am.Meterol.Soc, Portland, Oreg*.

Parthasarathy, B., A. A. Munot, and D. R. Kothawale, 1994: All India monthly and seasonal rainfall series: 1871-1993. *Theor. Appl. Climatol.*, **49**, 217–224.

Rajendran, K., A. Kitoh, and O. Arakawa, 2004: Monsoon low-frequency intraseasonal oscillations and ocean-atmosphere coupling over the Indian Ocean. *Geophys. Res. Lett.*, **31**, L02,210,doi:10.1029/2003GL019,031.

Ramage, C. S., 1971: *Monsoon Meteorology*. vol. 15 of *International Geophysics Series*, Academic Press.

Reynolds, R. W., and T. M. Smith, 1994: Improved global sea surface temperature analyses using optimum interpolation. *J. Climate*, **7**, 929–948.

Rosmond, T. E., 1992: The design and testing of the navy operational global atmospheric system. *Wea. Forecasting*, **7**, 262–272.

Shin, D. W., T. E. LaRow, and S. Cocke, 2003: Convective scheme and resolution impacts on seasonal precipitation forecasts. *Geophys. Res. Lett.*, **30**, 689,doi:10,1029/2003GL018,297.

Shukla, J., 1987: Interannual variability of monsoon. *Monsoons*, J. S. Fein and P. L. Stephens, Eds., Wiley and Sons, pp. 399–464.

Sikka, D. R., and S. Gadgil, 1980: On the maximum cloud zone and the ITCZ over Indian longitude during southwest monsoon. *Mon. Wea. Rev.*, **108**, 1840–1853.

Sperber, K. R., and T. N. Palmer, 1996: Interannual tropical rainfall variability in general circulation model simulations associated with atmospheric model intercomparison project. *J. Climate*, **9**, 2727–2750.

Sperber, K. R., et al., 2001: Dynamic seasonal predictability of the Asian summer monsoon. *Mon. Wea. Rev.*, **129**, 2226–2248.

Waliser, D., et al., 2003: AGCM simulations of intraseasonal variability associated with the Asian summer monsoon. *Climate Dyn.*, **21**, 423–446.

Wang, B., I.-S. Kang, and J.-Y. Lee, 2004: Ensemble simulations of Asian-Australian monsoon variability by 11 AGCMs. *J. Climate*, **17**, 803–818.

Webster, P. J., V. O. Magana, T. N. Palmer, J. Shuka, R. T. Tomas, M. Yanai, and T. Yasunari, 1998: Monsoons: Processes, predictability and the prospects of prediction. *J. Geophys. Res.*, **103(C7)**, 14,451–14,510.

Xie, P., and P. A. Arkin, 1997: Global precipitation: A 17-year monthly analysis based on guage observations, satellite estimates and numerical model outputs. *Bull. Amer. Meteor. Soc.*, **78**, 2539–2558.

Yasunari, T., 1979: Cloudiness fluctuation associated with the Northern Hemisphere summer monsoon. *J. Meteor. Soc. Japan*, **57**, 227–242.

Yasunari, T., 1980: A quasi-stationary appearance of 30-40 day period in the cloudiness

fluctuation during summer monsoon over India. *J. Meteor. Soc. Japan*, **58**, 225–229.

Zhang, G. J., and N. A. McFarlane, 1995: Sensitivity of climate simulations to the parametrizations of cumulus convection in the Canadian Climate Centre general circulation model. *Atmos.-Ocean*, **33**, 407–446.

Printed May 17, 2004.

Table Captions

TABLE: 1. (left panel) Cross correlation between the different monsoon indices calculated from model. (right panel) Cross correlation between the different monsoon indices calculated from model simulations with that calculated from observed data sets.

Figure Captions

FIG. 1. Ensemble mean JJAS seasonal mean precipitation (mm.day^{-1}) simulated by FSUGSM using different convection schemes. Seasonal mean precipitation is calculated as the mean of ten ensembles with different initial conditions.

FIG. 2. (a,b) 21-year climatological JJAS and DJF seasonal mean precipitation (mm.day^{-1}) derived from model simulations. (c,d) Same as in (a,b) but from observations (CMAP).

FIG. 3. 21-year climatological JJAS seasonal mean of (a) 850hPa winds and (b) 200hPa winds (ms^{-1}) derived from model simulations. (c,d) Corresponding observed winds from NCEP/NCAR Reanalysis.

FIG. 4. Climatological annual mean evolution of monsoon indices. Indices are defined in section.3

FIG. 5. (a) Vertically averaged (600hPa to 200hPa) temperature calculated from model simulations (b) Same as (a) but from NCEP/NCAR Reanalysis. Solid line indicates vertically averaged temperature over the northern latitudes (30°-130°E,10°-40°N) while the dotted line indicates the vertically averaged temperature over the southern latitudes (30°-130°E,30°S-10°N).

FIG. 6. An example showing power spectrum of simulated precipitation and zonal winds at 850hPa (U_{850}). Precipitation anomalies are averaged over 85°-95°E and 10°-15°N and U_{850} anomalies are averaged over 55°-65°E and 5°-10°N. Dashed line indicates 95% confidence limit.

FIG. 7. (a) Intraseasonal Variance of 10-90 day filtered June-September precipitation anomalies ($mm^2.day^{-2}$) from the model. (b) Same as (a) but from CMAP. (c) Intraseasonal Variance of 10-90 day filtered June-September zonal wind anomalies at 850hPa (m^2s^{-2}) from the model. (d) Same as (c) but from NCEP/NCAR Reanalysis.

FIG. 8. (a) Latitude versus lags (days) plot of 70°-95°E averaged filtered precipitation anomalies ($mm.day^{-1}$) derived from model simulations. (b) Same as (a) but for CMAP. (c) Same as (a) but for zonal wind anomalies at 850hPa (ms^{-1}). (d) Same as (c) but from NCEP/NCAR Reanalysis.

FIG. 9. (a) Active minus break precipitation composites ($mm.day^{-1}$) from the model and (b) from CMAP. Composites are calculated from 10-90 day filtered precipitation anomalies based on normalized EIMR.

FIG. 10. Same as Fig.9 but for 850hPa winds (ms^{-1}).

FIG. 11. Same as Fig.9 but for 200hPa winds (ms^{-1}).

FIG. 12. Different indices of monsoon interannual variability. (a) EIMR from model and CMAP. (b) Normalized EIMR, MH and KELLJ.

FIG. 13. (a) Interannual variance of JJAS seasonal mean precipitation anomalies ($mm^2.day^{-2}$) calculated from model simulations (b) Same as in (a) but for CMAP (c) Same as (a) but for zonal wind anomalies at 850hPa (m^2s^{-2}) (d) Same as in (c) but from NCEP/NCAR Reanalysis.

FIG. 14. Strong minus weak composites of seasonal mean precipitation and wind anomalies. (a) Model Precipitation (b) CMAP Precipitation (c) 850hPa winds from model (d) 850hPa winds from NCEP (e) 200hPa winds from model (f) 200hPa winds from NCEP. Strong/Weak monsoon years are identified based on normalized EIMR.

FIG. 15. (a) Correlation coefficients between JJAS Niño-3 sea surface temperature anomalies (SSTA) and JJAS model precipitation (b) Same as (a) but with respect to CMAP precipitation.

FIG. 16. Hadley and Walker circulation changes associated with ENSO. (a) JJAS 70°-95°E averaged meridional wind (v) and pressure vertical velocity (w x -0.5×10^4) anomalies at different levels plotted as a function of latitude. (b) Same as (a) but from NCEP (w x -0.1×10^3) (c)JJAS 5°S-5°N averaged zonal wind (u) and pressure vertical velocity (w x -0.2×10^5) anomalies at different levels plotted as a function of longitude. (d) Same as (c) but from NCEP (w x -0.14×10^3).

Tables

Table of Correlation:

Model / Model	EIMR	MH	KELLJ
EIMR	1		
MH	0.5034	1	
KELLJ	0.8549	0.5963	1

Model / Observed	EIMR	MH	KELLJ
EIMR	0.0766	-0.1707	-0.1806
MH	0.1101	-0.2819	-0.0755
KELLJ	0.59	0.2785	0.4371

TABLE 1. (left panel) Cross correlation between the different monsoon indices calculated from model. (right panel) Cross correlation beteen the different monsoon indices calculated from model simulations with that calculated from observed data sets.

Figures

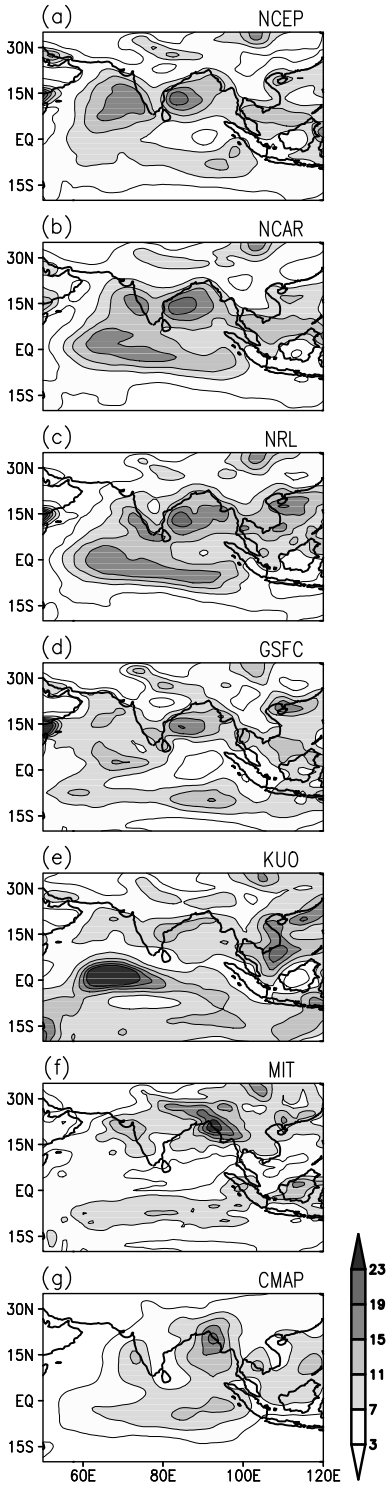

FIG. 1. Ensemble mean JJAS seasonal mean precipitation (mm.day^{-1}) simulated by FSUGSM using different convection schemes. Seasonal mean precipitation is calculated as the mean of ten ensembles with different initial conditions.

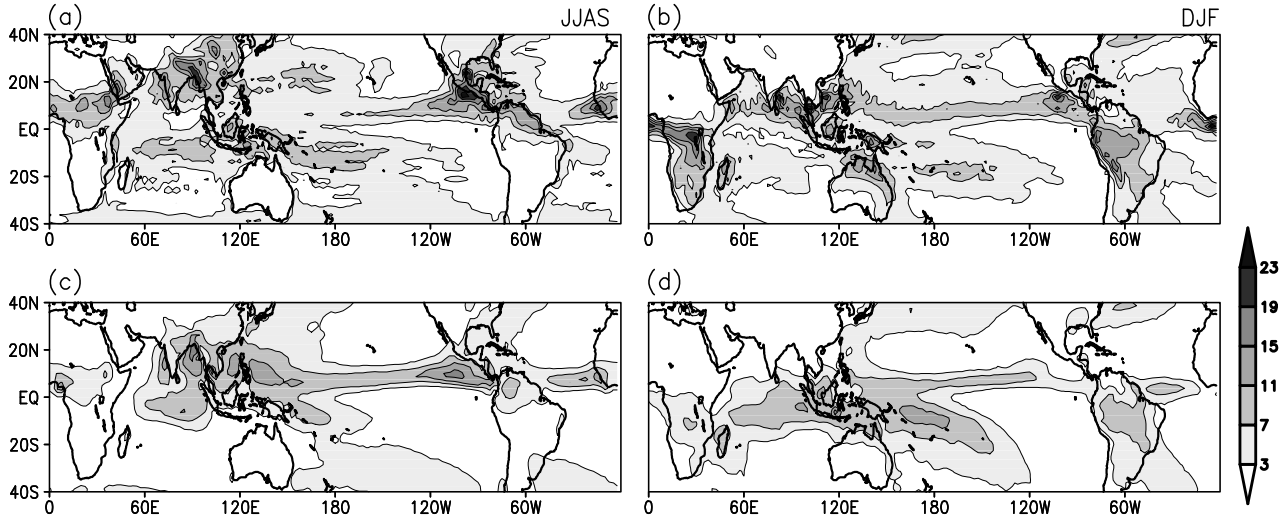

FIG. 2. (a,b) 21-year climatological JJAS and DJF seasonal mean precipitation (mm.day^{-1}) derived from model simulations. (c,d) Same as in (a,b) but from observations (CMAP).

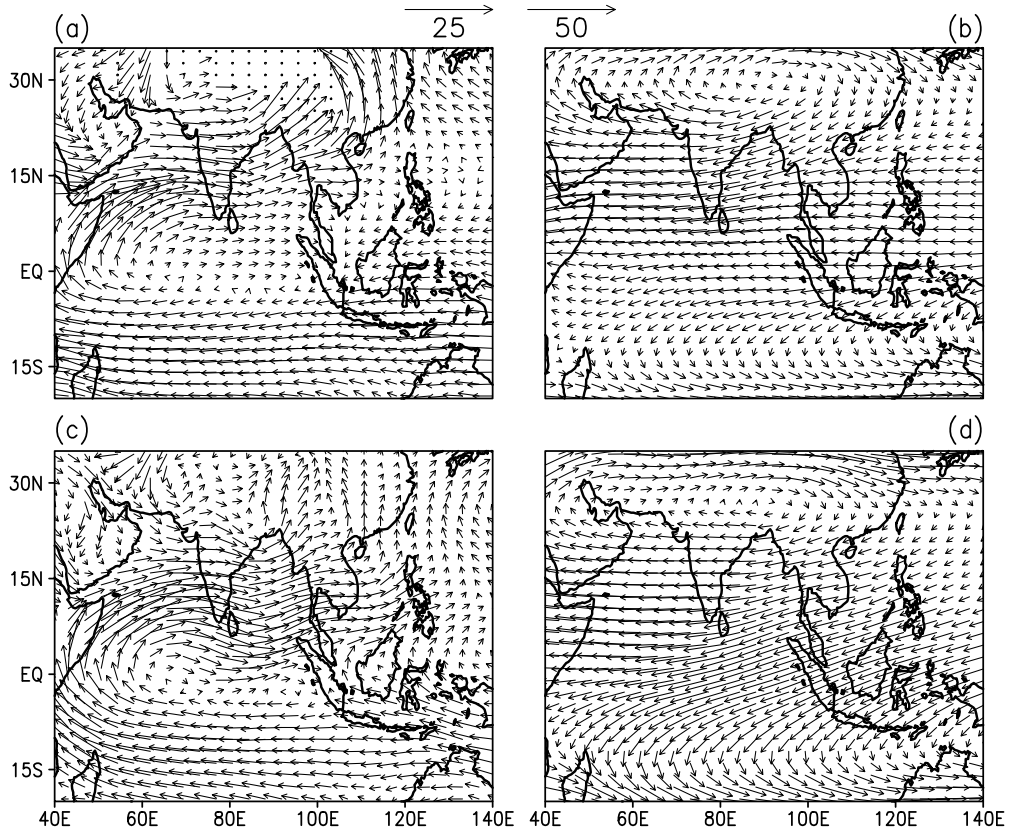

FIG. 3. 21-year climatological JJAS seasonal mean of (a) 850hPa winds and (b) 200hPa winds (ms^{-1}) derived from model simulations. (c,d) Corresponding observed winds from NCEP/NCAR Reanalysis.

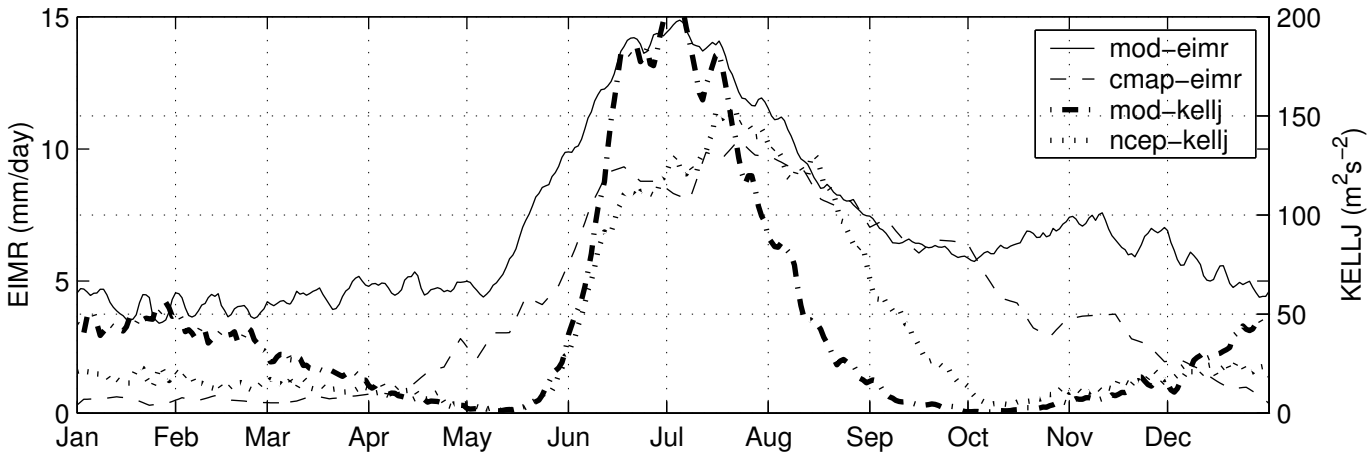

FIG. 4. Climatological annual mean evolution of monsoon indices. Indices are defined in section.3

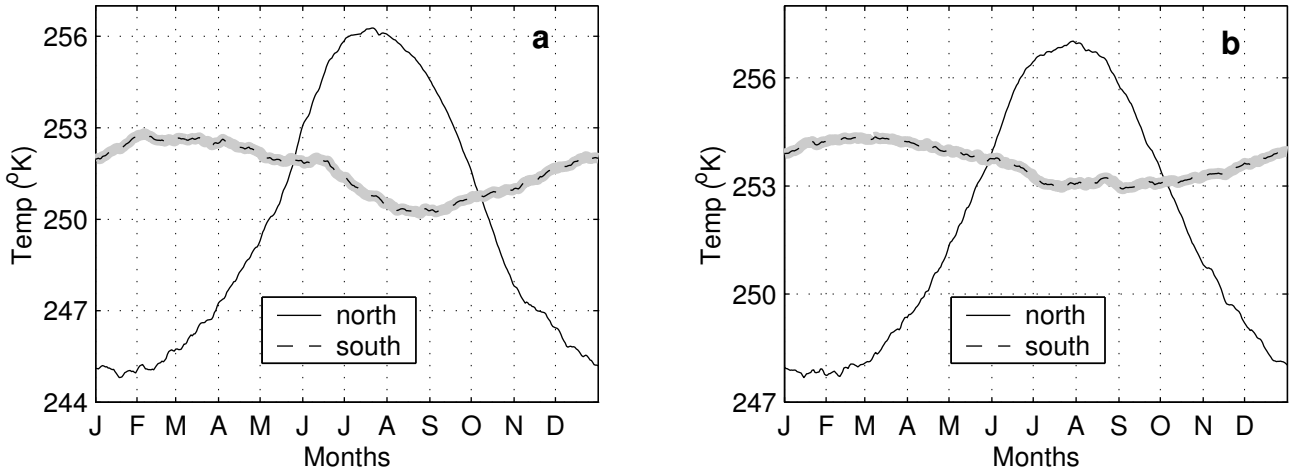

FIG. 5. (a) Vertically averaged (600hPa to 200hPa) temperature calculated from model simulations (b) Same as (a) but from NCEP/NCAR Reanalysis. Solid line indicates vertically averaged temperature over the northern latitudes (30°-130°E,10°-40°N) while the dotted line indicates the vertically averaged temperature over the southern latitudes (30°-130°E,30°S-10°N).

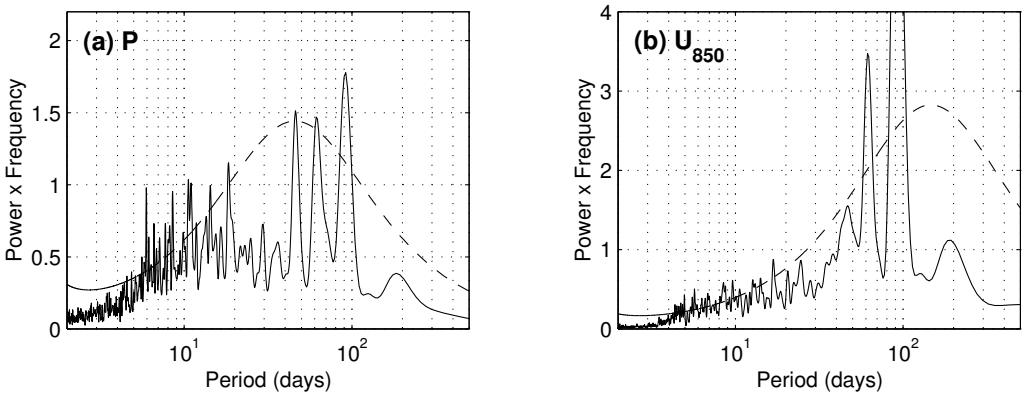

FIG. 6. An example showing power spectrum of simulated precipitation and zonal winds at 850hPa (U_{850}). Precipitation anomalies are averaged over 85°-95°E and 10°-15°N and U_{850} anomalies are averaged over 55°-65°E and 5°-10°N. Dashed line indicates 95% confidence limit.

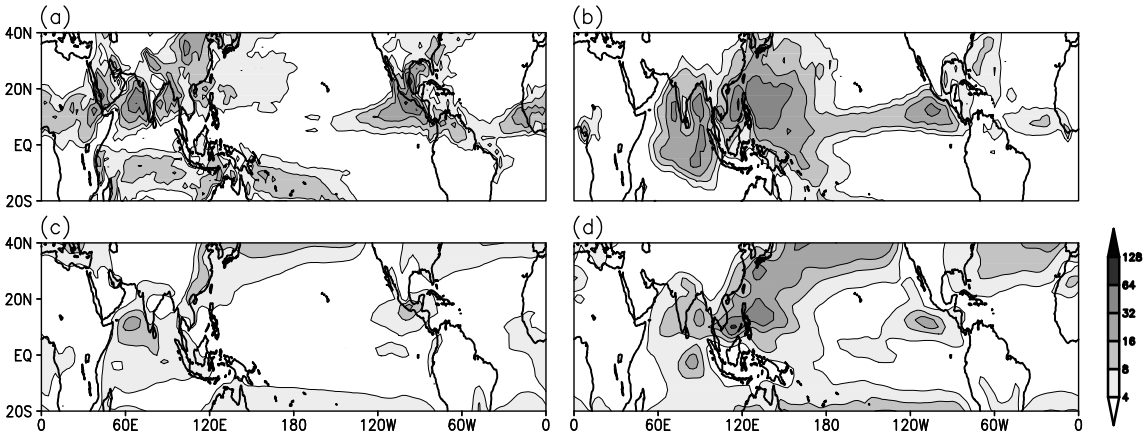

FIG. 7. (a) Intraseasonal Variance of 10-90 day filtered June-September precipitation anomalies ($mm^2.day^{-2}$) from the model. (b) Same as (a) but from CMAP. (c) Intraseasonal Variance of 10-90 day filtered June-September zonal wind anomalies at 850hPa (m^2s^{-2}) from the model. (d) Same as (c) but from NCEP/NCAR Reanalysis.

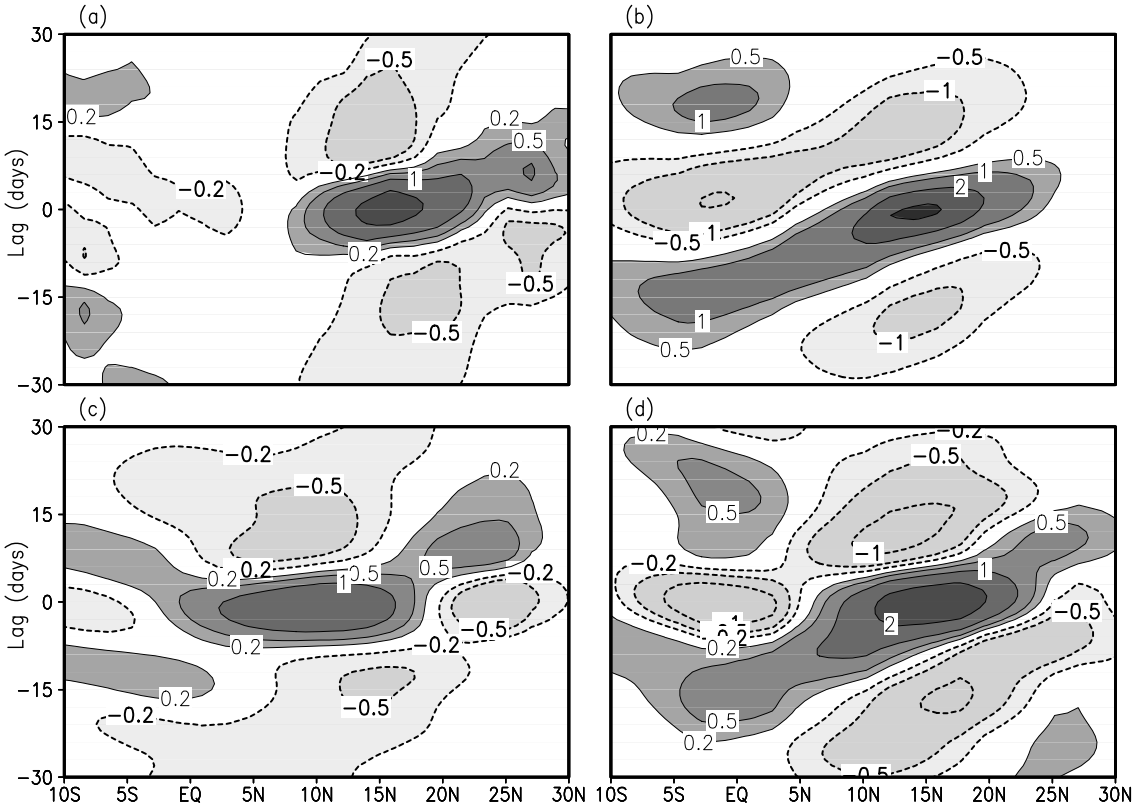

FIG. 8. (a) Latitude versus lags (days) plot of 70°-95°E averaged filtered precipitation anomalies (mm.day^{-1}) derived from model simulations. (b) Same as (a) but for CMAP. (c) Same as (a) but for zonal wind anomalies at 850hPa (ms^{-1}). (d) Same as (c) but from NCEP/NCAR Reanalysis.

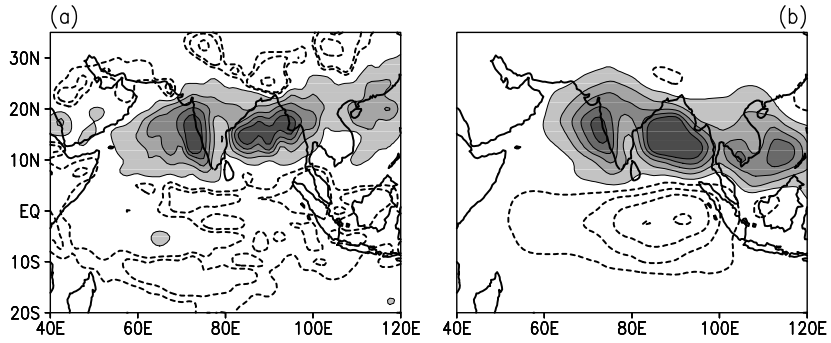

FIG. 9. (a) Active minus break precipitation composites (mm.day^{-1}) from the model and (b) from CMAP. Composites are calculated from 10-90 day filtered precipitation anomalies based on normalized EIMR.

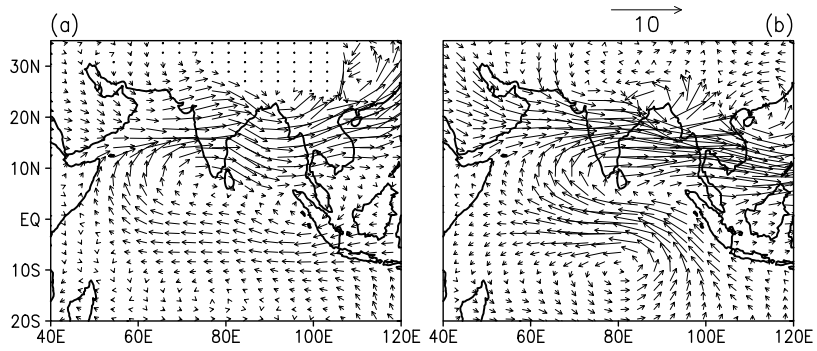

FIG. 10. Same as Fig.9 but for 850hPa winds (ms^{-1}).

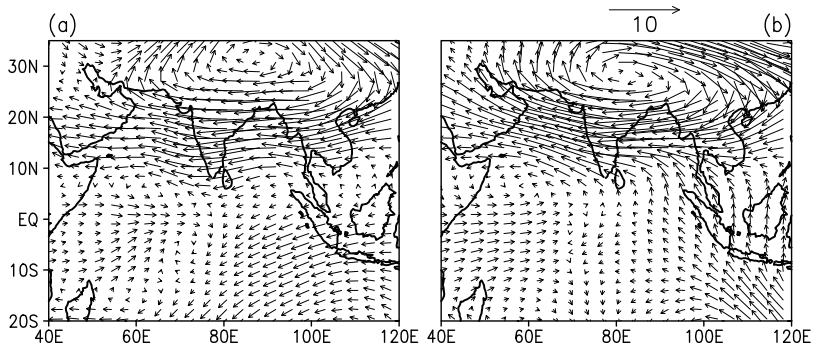

FIG. 11. Same as Fig.9 but for 200hPa winds (ms^{-1}).

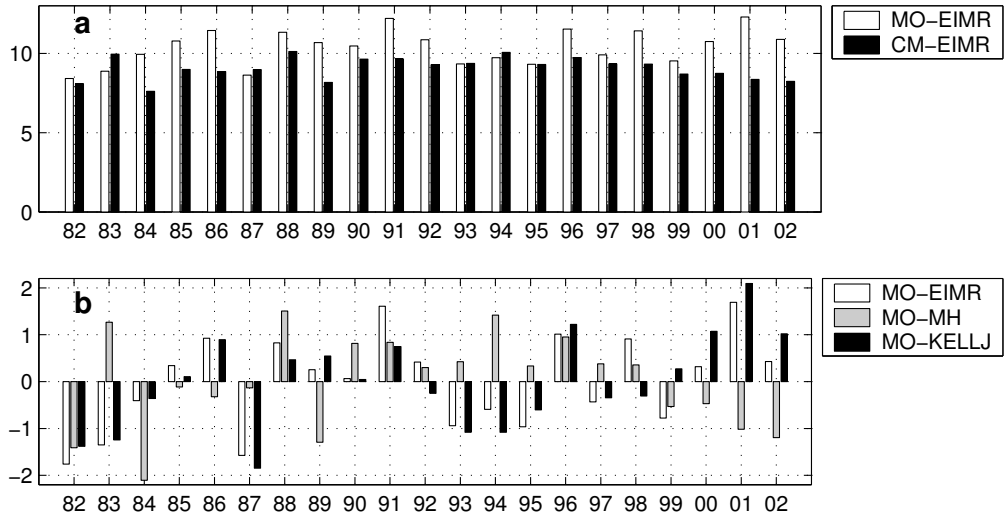

FIG. 12. Different indices of monsoon interannual variability. (a) EIMR from model and CMAP. (b) Normalized EIMR, MH and KELLJ.

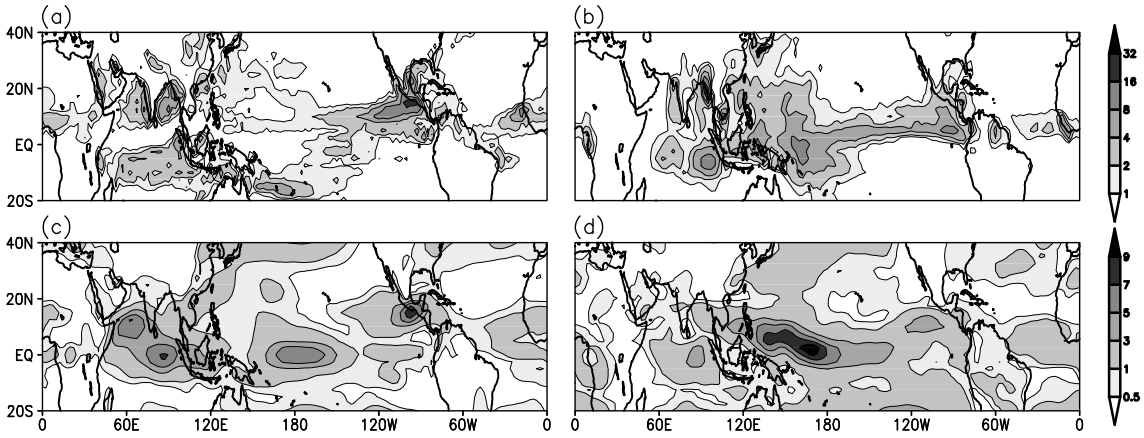

FIG. 13. (a) Interannual variance of JJAS seasonal mean precipitation anomalies ($mm^2.day^{-2}$) calculated from model simulations (b) Same as in (a) but for CMAP (c) Same as (a) but for zonal wind anomalies at 850hPa (m^2s^{-2}) (d) Same as in (c) but from NCEP/NCAR Reanalysis.

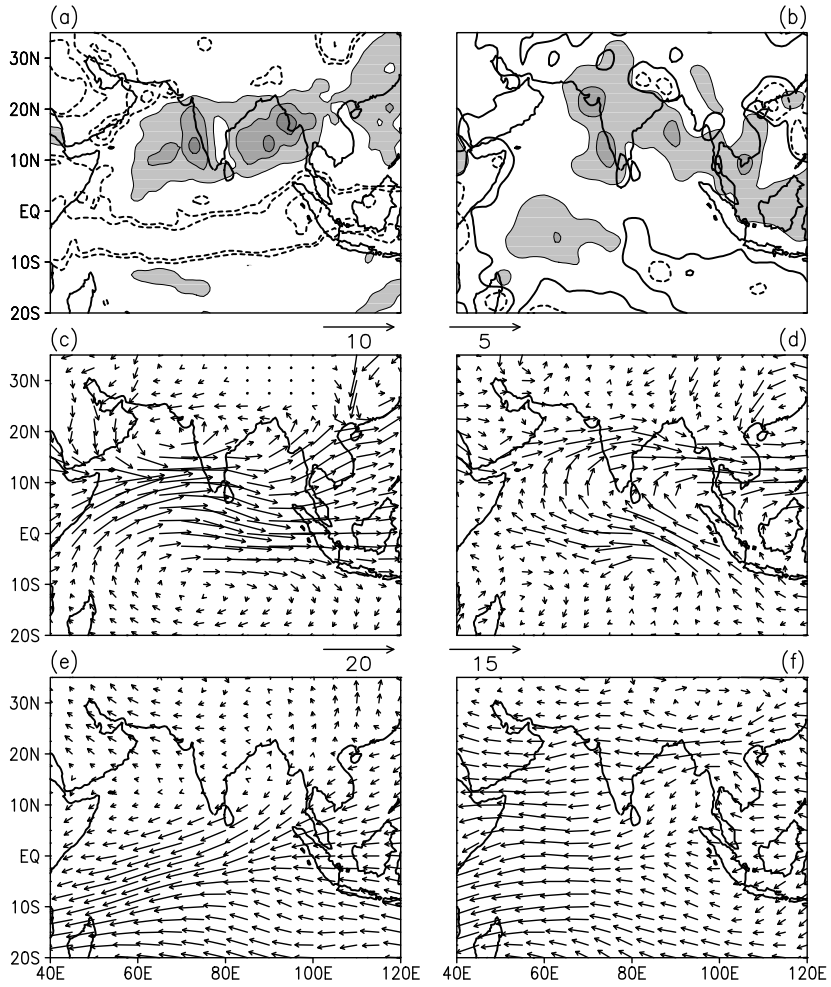

FIG. 14. Strong minus weak composites of seasonal mean precipitation and wind anomalies. (a) Model Precipitation (b) CMAP Precipitation (c) 850hPa winds from model (d) 850hPa winds from NCEP (e) 200hPa winds from model (f) 200hPa winds from NCEP. Strong/Weak monsoon years are identified based on normalized EIMR.

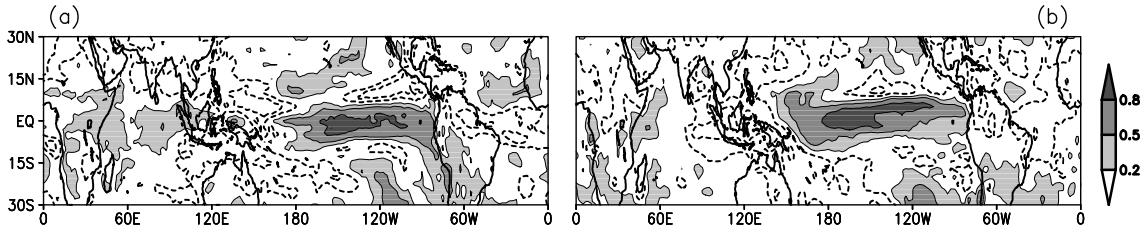

FIG. 15. (a) Correlation coefficients between JJAS Niño-3 sea surface temperature anomalies (SSTA) and JJAS model precipitation (b) Same as (a) but with respect to CMAP precipitation.

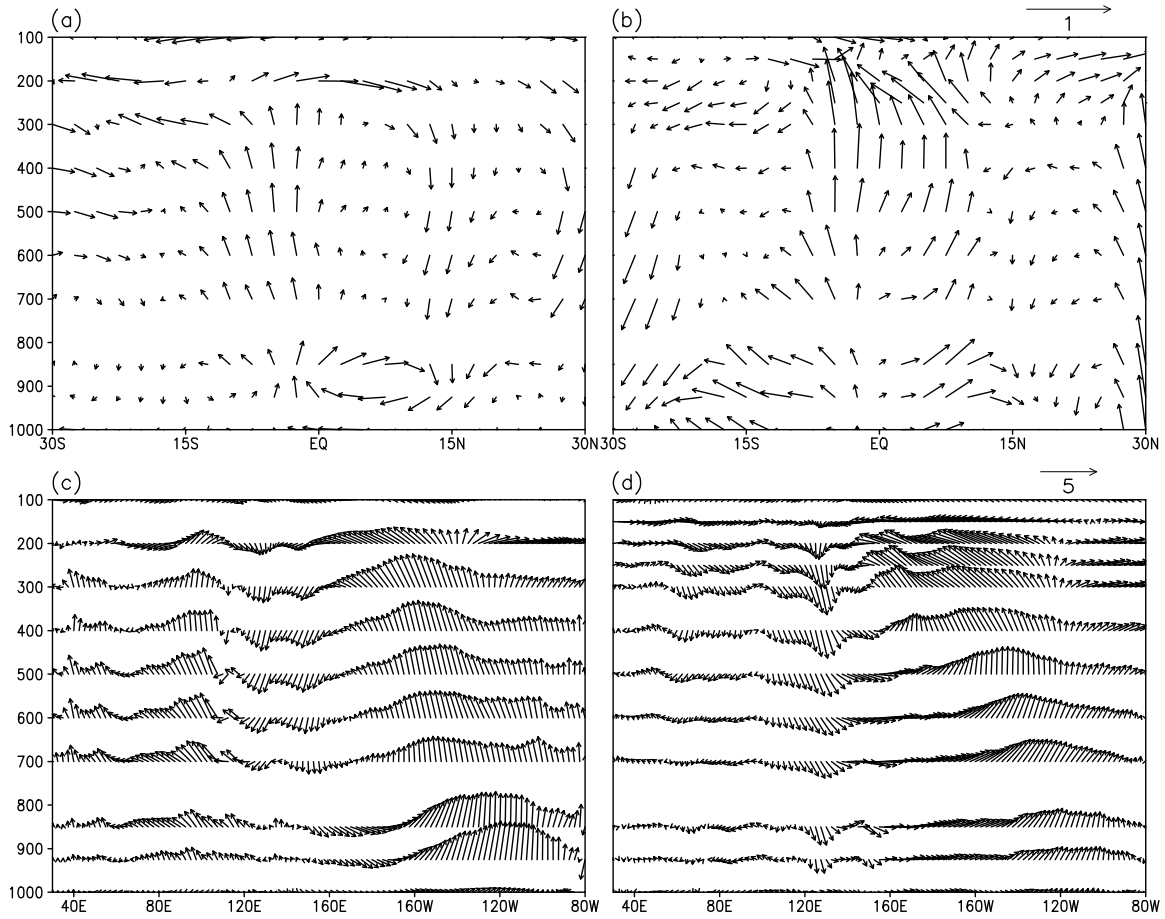

FIG. 16. Hadley and Walker circulation changes associated with ENSO. (a) JJAS 70°-95°E averaged meridional wind (v) and pressure vertical velocity (w x -0.5×10^4) anomalies at different levels plotted as a function of latitude. (b) Same as (a) but from NCEP (w x -0.1×10^3) (c)JJAS 5°S-5°N averaged zonal wind (u) and pressure vertical velocity (w x -0.2×10^5) anomalies at different levels plotted as a function of longitude. (d) Same as (c) but from NCEP (w x -0.14×10^3).